International Journal of Waste Resources

OPEN ACCESS Freely available online

Research Article

Facile Synthesis and Characterization of rGO Decorated $NiFe_2O_4$ Nano-composite Obtained from Waste Ni-Cd/Ni-MH Batteries

Mylarappa M[1]*, Venkata Lakshmi V[2], Kantharaju S[1]

[1]*Department of Chemistry, Sri Jagadguru Renukacharya College of Science, Arts and Commerce, Bangaluru-560009, Karnataka, India;* [2]*Research Centre, Department of Chemistry, AMC Engineering College, Bengaluru-560083, Karnataka, India*

ABSTRACT

The present study revealed the $NiFe_2O_4$/rGO composite synthesized from Ni-Cd/Ni-MH spent by hydrothermal method. The obtained $NiFe_2O_4$ nano particles was dispersed effectively on reduced graphene oxide and the obtained composite was subjected to X-Ray powder diffraction (XRD) to know the particle crystallinity, size and structural aspects. The nano sized $NiFe_2O_4$ and $NiFe_2O_4$/rGO nano composite were exposed to study the surface particle morphology by using Field emission Scanning Electron Microscopy (FESEM). The elements present in the sample was analyzed by using Energy Dispersive X-Ray analysis (EDX), the functional groups identification was done by Fourier Transform Infrared Spectrometer (FTIR) and the thermal stability was studies by using Thermogravimetry analysis.

Keywords: Waste battery; $NiFe_2O_4$; $NiFe_2O_4$/rGO; Characterization; Thermal analysis

INTRODUCTION

Nickel ferrite ($NiFe_2O_4$) nanocrystalline is one of the most vital ferrites among alternative ferrites from the spent battery because of most favorable uses in Ferro fluids, gas sensors, storage devices, catalysts and microwave devices [1-7]. Recently, extensive consideration has been paid on $NiFe_2O_4$ with variable size, morphology and shape as well analogous applications were studied [8,9]. In the synthesis of $NiFe_2O_4$, both chemical and physical methods have been established with different surface morphology. Compared to physical methods, the chemical methods have benefits such as large scale production, low cost and reaction taking place at very low temperature. The nano structured $NiFe_2O_4$ has been prepared by different process like sonochemical, polymeric precursor, mechanical alloying, hydrothermal, and co-precipitation methods [10-14].

The literature shows that a few works on the surface morphology controlled preparation of the $NiFe_2O_4$ nano particles. Newly, fabricated $NiFe_2O_4$ nano sheets using chemical method by Gunjakar et al. [15]. Chu et al. synthesized nano cubes and nanorods of $NiFe_2O_4$ through hydrothermal process [16]. Zhang et al. via polyethylene glycol method prepared $NiFe_2O_4$ nano particles [17], the hollow sphere $NiFe_2O_4$ nano rods and their magnetic properties was studied by Chen L et al. [18]. Also several studies have concentrated on the synthesis of spinel nano ferrites because of their quantum confinement effects, both chemical and physical properties and their surface effects.

The nano $NiFe_2O_4$ have AB_2O_4 structure. In this structure, O specifies the oxygen anion site and A and B shows tetrahedral and octahedral cation sites [19]. The nickel ions (Ni^{+2}) are located in B sites and iron ions (Fe^{3+}) are equally dispersed between A and B sites. It is well known that combined metal oxide nano particles are seemly very attractive to making the electrode materials due to their controlling morphology and size, high surface energy, attractive structural, magnetic and electronic activities, which improve their catalytic performance [20-22].

In the synthesis of nano $NiFe_2O_4$, reduced graphene oxide (rGO) was selected as solid subsidiary material to keep the nano $NiFe_2O_4$ from aggregation. The rGO based nano composite materials will have increased electrochemical performance like reversibility, capacitive action and cycling stability. The rGO doped nano composite have been widely used as anodes for rechargeable batteries and some recent studies shows the production of rGO based metal-oxide anode materials have equitably good development [23,24]. For example, $MgFe_2O_4$/rGO composites was displayed excellent cycling stability and rate capability synthesized by Zhang et al. and SnO_2/rGO nano hybrid exhibited that electrochemical Na-storage

***Corresponding to**: Mylarappa M, Department of Chemistry, Sri Jagadguru Renukacharya College of Science, Arts and Commerce, Bangaluru-560009, Karnataka, India, Tel: +91-9742413751; E-mail: mylu4mkallihatti@gmail.com

Received: July 25, 2020; **Accepted:** August 27, 2020; **Published:** September 03, 2020

Citation: Mylarappa M, Venkata Lakshmi V, Kantharaju S (2020) Facile Synthesis and Characterization of rGO Decorated $NiFe_2O_4$ Nano-composite Obtained from Waste Ni-Cd/Ni-MH Batteries, Int J Waste Resour 10: 385. doi: 10.35248/2252-5211.20.10.385.

activity enhanced due to amalgamation of reduced graphene oxide [25].

The synthesis and structural aspects of $NiFe_2O_4$/rGO nano composite obtained from waste Ni-Cd/Ni-MH batteries by hydrothermal process are not yet described. The current study revealed the facile synthesis of nickel ferrite from waste batteries and the obtained $NiFe_2O_4$ was adsorbed on the surface of reduced graphene oxide (rGO) via hydrothermal method.

EXPERIMENTAL METHODS

Materials and Methods

The list of chemicals, specifications and suppliers names were employed in this work as indicated in Table 1. The hydrometallurgical method is adapted for the synthesis and structural aspects of rGO doped nickel ferrite nano composite from spent Ni-Cd/Ni-MH batteries.

Synthesis of $NiFe_2O_4$ from Waste Batteries

The leached battery powder which obtained from waste Ni-Cd/Ni-MH batteries taken in a two necked round bottom flask about 1 g and add 100 ml of 3 M sulphuric acid (H_2SO_4) to dissolve Ni and Cd ions in the powder. When the cations were dissolve with acid, add stoichiometric amount of Mohr's salt as iron source to solution with constant stirring. The obtained mixture was subjected to analyze the P^H of the solution by using sodium hydroxide (NaOH) solution. The reaction mixture was performed at constant agitation speed of 250 rpm and proceeded at 100°C for 60 min, a brown colored precipitate was obtained. The obtained precipitate was dried at 200°C for 24 hours.

Synthesis of $NiFe_2O_4$/rGO Nano-Composite

The reduced graphene was added about 1 g in a 250 ml beaker containing 100 ml of distilled water and 1 g of synthesized nano $NiFe_2O_4$ obtained from above taken in another beaker separately using ultra-sonication for better dispersion for 30 min. The well dispersed $NiFe_2O_4$ nano particles was decanted into the solution containing rGO in water with constant stirring. The entire mixture was maintained constant speed at 100°C for one hour. The obtained $NiFe_2O_4$/rGO nano composite was filtered, dried and washed. The precipitate was kept in oven for 24 hours at 100°C. The Flow chart and illustration of synthesis of $NiFe_2O_4$/rGO Nano composite as shown below Figure 1.

Table 1: list of chemicals, specifications and suppliers.

Materials	Specifications	Suppliers
Waste batteries	AA, and AAA	different manufactures
Oxalic acid di-hydrate $HO_2CCO_2H \cdot 2H_2O$	Molar mass: 192.16 g/mol	Merck, Bangalore, India
Citric acid $(C_6H_8O_7)$	Molecular wt.: 126.07 g/mol	Merck
Sulphuric acid (H_2SO_4)	Molecular wt.: 39.9 g/mol	Merck
Sodium Hydroxide (NaOH)	Molecular wt. : 40 g/mol	Merck
Reduced graphene oxide (rGO)	Carbon purity :> 99%, Thickness 3-6 nm.	United Nanotech Innovations Pvt. Ltd. Bangalore
Ferrous sulphate $(FeSO_4.7H_2O)$	Molar mass: 151.9 g/mol	Merck, Bangalore, India

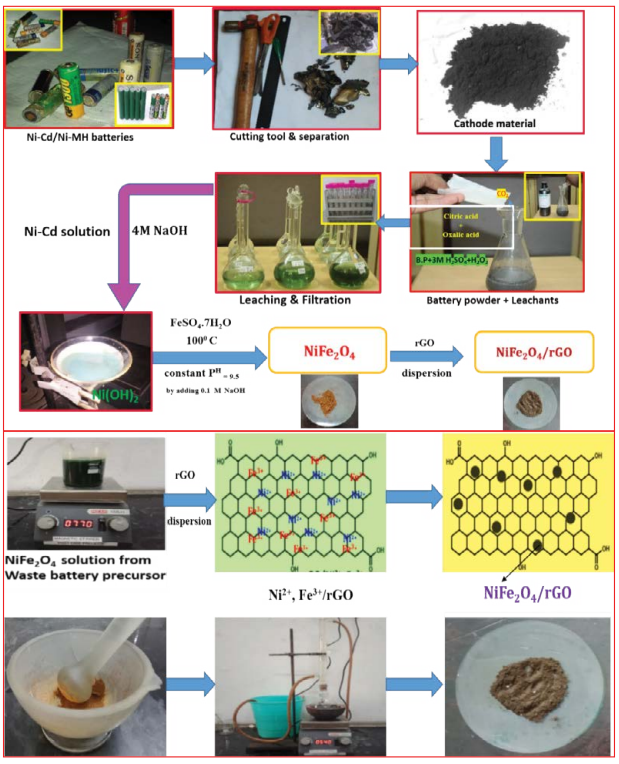

Figure 1: Flow chart and illustration of synthesis of $NiFe_2O_4$/rGO Nano composite.

RESULTS AND DISCUSSIONS

X-Ray Diffraction Studies

X-Ray diffraction (XRD) spectra of $NiFe_2O_4$ and $NiFe_2O_4$/rGO nano composite are shown in Figure 2. In Figure 2a, the measured average crystallite size of $NiFe_2O_4$ nanoparticle was about 9 nm and the graphic representation of a $NiFe_2O_4$ unit cell is presented as an introduced image in Figure 2a. The diffraction peaks of $NiFe_2O_4$ which indicated the formation of crystalline phase of $NiFe_2O_4$ and broadening of the peaks were confirmed the nano crystalline nature of the powder. In Figure2b, the particle size of $NiFe_2O_4$ nano particle and $NiFe_2O_4$/rGO nanocomposites was found to be 9 nm and 13.4 nm respectively by using the Scherrer's equation. In $NiFe_2O_4$/rGO nanocomposites the peak intensity (220) was disappear completely recommending that reducing crystal size of $NiFe_2O_4$, which reveals the growth of $NiFe_2O_4$ particles were essentially restricted after the fusing of rGO [26]. The extra peaks at about 27°, 29° and 46° are observed in Figure 2a were due to the contamination of the sample or that my occur during the leaching process of the waste batteries.

We observed that, the peak intensities of $NiFe_2O_4$/rGO nanocomposites compared to $NiFe_2O_4$ decreases with increase in average particle size and doped rGO will decreased intensity peak, which shows the growth of $NiFe_2O_4$ was controlled after the doping of rGO dispersion. The Williamson and Hall method and Scherrer's equation was employed to calculate the particle sizes of $NiFe_2O_4$ and $NiFe_2O_4$/rGO nano composite. According to Williamson and Hall, when lattice micro stain and domain were all together concurrently working their mutual effects provides the final line broadening of full width half maximum (FWHM) in which the sum of lattice distortion and particle grain size. The following equation gives a straight line between β cosθ and 4sinθ where ε is associated strain with nano composite.

$$cos\theta = \varepsilon(4sin\theta) + \frac{\lambda}{D} \quad (1)$$

From the above equation, the average crystalline size (D) is measured by the intercept $\frac{0.90\lambda}{D}$ and strain (ε) was calculated by the slope of the line obtained from the graph. The results obtained from the equation were analogous to the particle size calculated from the Scherrer's equation. Particle size and other structural parameters of $NiFe_2O_4$ and $NiFe_2O_4$/rGO as indicated in Table 2. The density and stacking fault were calculated by the following equations.

$$\delta = \frac{1}{D^2} \quad (2)$$

$$\varepsilon = \frac{\beta cos\theta}{4} \quad (3)$$

$$SF = \frac{2\pi^2}{45\sqrt{3}\,tan\theta} \quad (4)$$

Field Emission Scanning Electron Microscopy

The field emission scanning electron microscopy (FESEM) was used to analyze the surface morphology images of $NiFe_2O_4$ and $NiFe_2O_4$/rGO nano composite as shown in the Figures 3a-3d. The surface morphology of particles are composed of various quadrangular shape with 1μm and 2 μm as indicated in Figures 3a and 3b. In Figures 3c and 3d, clearly shows that when reduced graphene was dispersed in the ferrite, The $NiFe_2O_4$ can be spread on the surface of nano ferrite forming $NiFe_2O_4$/rGO nano composite and the morphology of the particles are well distributed and some have little aggloromation as shown in the Figures 3c and 3d.

EDAX Analysis

From elemental analysis data, observed that C, Ni, Fe and O peaks, which confirms the purity of our synthesized sample. The chemical composition of $NiFe_2O_4$ and rGO/$NiFe_2O_4$ nano composite was indicated in Table 2. The qualitative analysis of C, Ni, Fe and O in the $NiFe_2O_4$ and $NiFe_2O_4$/rGO nanocomposites are determined by using EDX analysis as shown in Figures 4a and 4b. The elemental composition of $NiFe_2O_4$ is composed of 20.45% oxygen, 7.70% carbon, 2.27% Nickel and 21.69% iron respectively. Similarly in Figure 4b, the chemical composition of $NiFe_2O_4$/rGO is consist of 26.0 % oxygen, 10.0% carbon, 2.59% Nickel and 21.69% iron respectively.

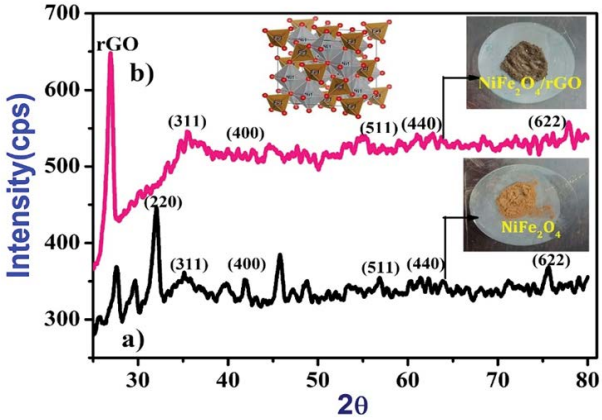

Figure 2: XRD spectra of a) $NiFe_2O_4$ and b) $NiFe_2O_4$/rGO nano composite.

Table 2: Particle size and other structural parameters of $NiFe_2O_4$ and $NiFe_2O_4$/rGO.

Name of the sample	FWHM (rad)	Crystalline Size (nm)	Strain (ε)×10^{-3}	stacking fault SF	dislocation density (δ) (10^5 lin m^{-2})
$NiFe_2O_4$	1.28	9	0.27	0.321	0.0123
$NiFe_2O_4$/rGO	0.632	13.4	0.140	0.353	0.0055

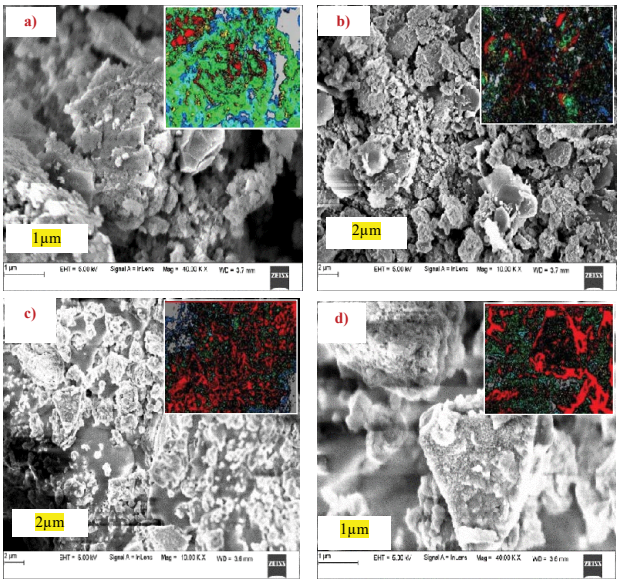

Figure 3: FESEM images of a) $NiFe_2O_4$ 1 µm b) $NiFe_2O_4$ 2µm c) NiFe2O4/rGO 1µm d) $NiFe_2O_4$/rGO 2 µm.

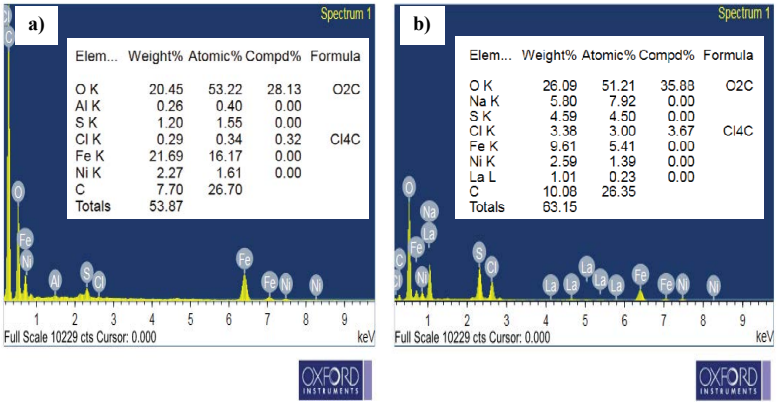

Figure 4: EDAX spectrum of a) $NiFe_2O_4$ b) $NiFe_2O_4$/rGO.

Fourier Transforms Infra-Red Spectrometer Studies

The functional groups attached for $NiFe_2O_4$ and $NiFe_2O_4$/rGO was performed by using Fourier transforms infra-red spectrometer (FT-IR). FTIR spectrum of $NiFe_2O_4$ $NiFe_2O_4$/rGO nano composite as shown in Figures 5a and 5b respectively.

In Figure 5a, the absorption frequency at 3290.2 cm^{-1} and 2169.2 cm^{-1} could be attributed to the symmetric vibration of -OH groups. The bands with peaks detected at 1087 cm^{-1} was assigned to O-H bending vibration. The absorption peaks near 1620 cm^{-1} and 608 cm^{-1} appeared in $NiFe_2O_4$ which are attributed to the skeletal vibration of metal-oxygen bonds of the $NiFe_2O_4$ particles. The vibration bands of Fe and Ni are found in the range of 1000–1200 cm^{-1} is the region of the vibrational bands of Fe_2O_3 in octahedral site and Ni–O in tetrahedral sites present in the samples [27-29]. In Figure 5b, the bands at about 21076 cm^{-1} and 1991.6 cm^{-1} are represented the stretching vibration of C=O and The bending vibration of H-O-H was assigned at 2107.6 cm^{-1}. The C-O bending vibration occur at absorbed frequency 108 7.1 cm^{-1} and peak 1622 cm^{-1} demonstrate the C=C stretching vibration of reduced graphene oxide sheets. The M-O bond absorbed at 579.9 cm^{-1} [30-32] and the rGO absorption bands resemble to the oxygen-containing functional groups are vanished in rGO doped nickel ferrite nano composite and the oxygen-containing functional groups almost vanished in $NiFe_2O_4$/rGO nano composite shows that oxygen-containing functional groups were almost removed in rGO dispersion reaction [33-35].

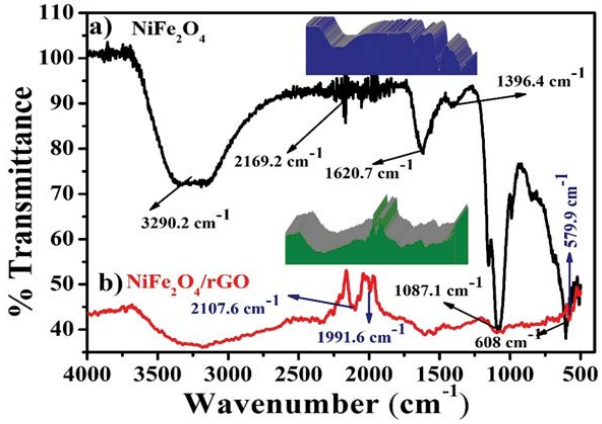

Figure 5: FTIR spectrum of a) $NiFe_2O_4$ b) $NiFe_2O_4$/rGO nano composite.

Thermogravimetry Analysis

The TGA of $NiFe_2O_4$ and $NiFe_2O_4$/rGO nano composite were studied by TGA and the results were shown in Figures 6a and 6b.

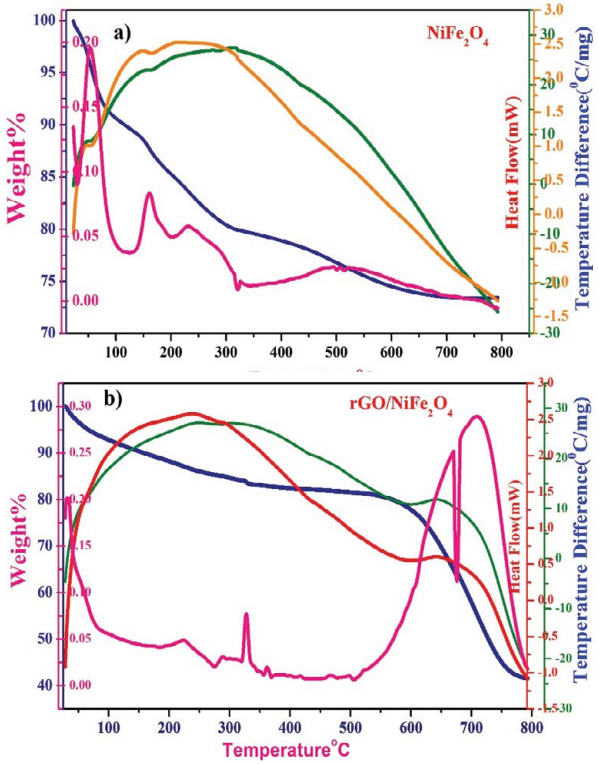

Figure 6: TGA of a) $NiFe_2O_4$ b) $NiFe_2O_4$/rGO nano composite.

In Figure 6a, The $NiFe_2O_4$ and $NiFe_2O_4$/rGO nano particles were The $NiFe_2O_4$ and $NiFe_2O_4$/rGO nano particles were prepared from spent battery as appeared in Figures 6a and 6b. In Figure 6a uncovers the $NiFe_2O_4$ nano particles has three separate warm disintegration steps. The main weight reduction stage in the temperature scope of 25°C-100°C, which was joined by an extremely little endothermic pinnacle is because of the loss of water particles in the $NiFe_2O_4$. The second region begins ~ 145^0 C and ends at 324°C with a weight loss of 80% which might be due to the initial breakdown of reactants. Almost no weight loss over ~708°C indicates the completion of thermal decomposition and formation of spinel ferrite [36].

In Figure 6b the rGO decorated nickel ferrite nano composite indicates three weight reduction forms. The weight loss below 100°C was removal of moisture in the sample. The weight reduction take place from 100 to 326°C, which caused by the destruction of oxygenated functional groups. Next a massive weight reduction happens between 326°C and 586°C. It tends to be dispersed to the ignition and disintegration of carbon molecule. The final exothermic phase was around 586°C and 796°C can be recognized for the rGO decorated $NiFe_2O_4$ composite and the weight loss occurred between 586°C and 796°C was indicating the conversion of reactants into the final products [37].

CONCLUSION

From this studies average particle sizes of $NiFe_2O_4$ and $NiFe_2O_4$/rGO composites of particle average size ranging from 9 to 13.4 nm were synthesized successfully from waste battery collection through hydrothermal method. The surface morphology of $NiFe_2O_4$ and $NiFe_2O_4$/rGO having quadrangular shape with NiFe2O4 nano particles are well covered on the rGO surface. The elements C, O, Ni and Fe were the main chemical constituents present in the sample which was confirmed by EDX analysis. From infrared analysis, the high frequency band at 579 and 608 cm^{-1} was corresponds to M-O bonds in $NiFe_2O_4$ and $NiFe_2O_4$/rGO nano composite. From Thermal studies, the sample $NiFe_2O_4$ nano particles can withstand the temperature up to 706°C and $NiFe_2O_4$/rGO nano composite up to 796.6°C respectively.

REFERENCES

1. Sugimoto M. The past, present, and future of ferrites. Journal of the American Ceramic Society. 1999;82(2):269-80.
2. Reddy CG, Manorama SV, Rao VJ. Semiconducting gas sensor for chlorine based on inverse spinel nickel ferrite. Sensors and Actuators B: Chemical. 1999;55(1):90-5.
3. Reddy CG, Manorama SV, Rao VJ. Preparation and characterization of ferrites as gas sensor materials. Journal of materials science letters. 2000;19(9):775-8.
4. Dube G, Darshane V. J, (1993) Mol Catal. 79:285-96.
5. Sousa MH, Hasmonay E, Depeyrot J, Tourinho FA, Bacri JC, Dubois E, et al. NiFe2O4 nanoparticles in ferrofluids: evidence of spin disorder in the surface layer. Journal of magnetism and magnetic materials. 2002;242:572-4.
6. Ramankutty CG, Sugunan S. Surface properties and catalytic activity of ferrospinels of nickel, cobalt and copper, prepared by soft chemical methods. Applied Catalysis A: General. 2001;218(1-2):39-51.
7. Šepelák V, Baabe D, Mienert D, Schultze D, Krumeich F, Litterst FJ, et al. Evolution of structure and magnetic properties with annealing temperature in nanoscale high-energy-milled nickel ferrite. Journal of Magnetism and Magnetic Materials. 2003 Feb 1;257(2-3):377-86.
8. Gunjakar JL, More AM, Gurav KV, Lokhande CD. Chemical synthesis of spinel nickel ferrite (NiFe2O4) nano-sheets. Applied Surface Science. 2008;254(18):5844-8.
9. Wang H, Zhang W, Zhang F, Cao Y, Su W. The effect of 3-aminopropyltrimethoxysilane on the formation of NiFe2O4/SiO2 nanocomposites. Journal of magnetism and magnetic materials. 2008;320(13):1916-20.
10. Yang JM, Tsuo WJ, Yen FS. Preparation of ultrafine nickel ferrite powders using mixed Ni and Fe tartrates. Journal of Solid State Chemistry. 1999;145(1):50-7.
11. Prasad S, Gajbhiye NS. Magnetic studies of nanosized nickel ferrite particles synthesized by the citrate precursor technique. Journal of Alloys and Compounds. 1998;265(1-2):87-92.
12. Chen DH, He XR. Synthesis of nickel ferrite nanoparticles by sol-gel method. Materials Research Bulletin. 2001 May 1;36(7-8):1369-77.
13. Liu C, Zou B, Rondinone AJ, Zhang ZJ. Chemical control of superparamagnetic properties of magnesium and cobalt spinel ferrite nanoparticles through atomic level magnetic couplings. Journal of the American Chemical Society. 2000 Jul 5;122(26):6263-7.
14. Zhou J, Ma J, Sun C, Xie L, Zhao Z, Tian H, et al. Low-Temperature Synthesis of NiFe2O4 by a Hydrothermal Method. Journal of the American Ceramic Society. 2005;88(12):3535-7.
15. Gunjakar JL, More AM, Gurav KV, Lokhande CD. Chemical synthesis of spinel nickel ferrite (NiFe2O4) nano-sheets. Applied Surface Science. 2008;254(18):5844-8.
16. Chu XF, Jiang DL, Zheng CM. The preparation and gas-sensing properties of NiFe2O4 nanocubes and nanorods. Sens. Actuators B. 2007;123(2):793-7.
17. Zhang DE, Zhang XJ, Ni XM, Zheng HG, Yang DD. Synthesis and characterization of NiFe2O4 magnetic nanorods via a PEG-assisted route. Journal of Magnetism and Magnetic Materials. 2005;292:79-82.
18. Chen L, Dai H, Shen Y, Bai J. Size-controlled synthesis and magnetic properties of NiFe2O4 hollow nanospheres via a gel-assistant

hydrothermal route. Journal of Alloys and Compounds. 2010;491(1-2):L33-8.

19. O'handley RC. Modern magnetic materials: principles and applications. Wiley; 2000.
20. Srivastava M, Singh J, Kuila T, Layek RK, Kim NH, Lee JH. Recent advances in graphene and its metal-oxide hybrid nanostructures for lithium-ion batteries. Nanoscale 7: 4820-68
21. Son DI, Yang HY, Kim TW, Park WI. Transparent and flexible ultraviolet photodetectors based on colloidal ZnO quantum dot/graphene nanocomposites formed on poly (ethylene terephthalate) substrates. Composites Part B: Engineering. 2015;69:154-8.
22. Tang Q, Chen M, Wang L, Wang G. A novel asymmetric supercapacitors based on binder-free carbon fiber paper@ nickel cobaltite nanowires and graphene foam electrodes. Journal of Power Sources. 2015;273:654-62.
23. Qin W, Li D, Zhang X, Yan D, Hu B, Pan L. ZnS nanoparticles embedded in reduced graphene oxide as high performance anode material of sodium-ion batteries. Electrochimica Acta. 2016;191:435-43.
24. Walter M, Zünd T, Kovalenko MV. Pyrite (FeS 2) nanocrystals as inexpensive high-performance lithium-ion cathode and sodium-ion anode materials. Nanoscale. 2015;7(20):9158-63.
25. Zhang Y, Xie J, Zhang S, Zhu P, Cao G, Zhao X. Ultrafine tin oxide on reduced graphene oxide as high-performance anode for sodium-ion batteries. Electrochimica Acta. 2015;151:8-15.
26. Shetty K, Lokesh SV, Rangappa D, Nagaswarupa HP, Nagabhushana H, Anantharaju KS, et al. Designing MgFe2O4 decorated on green mediated reduced graphene oxide sheets showing photocatalytic performance and luminescence property. Physica B: Condensed Matter. 2017;507:67-75.
27. Ren L, Qiu J, Wang S. Photovoltaic properties of graphene nanodisk-integrated polymer composites. Composites Part B: Engineering. 2013;55:548-57.
28. Guo L, Shen X, Meng X, Feng Y. Effect of Sm3+ ions doping on structure and magnetic properties of nanocrystalline NiFe2O4 fibers. Journal of Alloys and Compounds. 2010;490(1-2):301-6.
29. Tahir MB, Iqbal T, Hassan A, Ghazal S. Wet chemical co-precipitation synthesis of nickel ferrite nanoparticles and their characterization. Journal of Inorganic and Organometallic Polymers and Materials. 2017;27(5):1430-8.
30. Li Y, Zhang Z, Pei L, Li X, Fan T, Ji J, et al. Multifunctional photocatalytic performances of recyclable Pd-NiFe2O4/reduced graphene oxide nanocomposites via different co-catalyst strategy. Applied Catalysis B: Environmental. 2016;190:1-1.
31. Qiu Q, Chen Y, Xue J, Zhu J, Fu Y, He G, et al. One-step solvothermal synthesis of spherical spinel type NiFe2− xMnxO4-RGO as high-performance supercapacitor electrodes. Ceramics International. 2017 43(2):2226-32.
32. Qi F, Xu B, Chu W. Heterogeneous catalytic ozonation of phenacetin in water using magnetic spinel ferrite as catalyst: Comparison of surface property and efficiency. Journal of Molecular Catalysis A: Chemical. 2015;396:164-73.
33. Zhao Y, He G, Dai W, Chen H. High catalytic activity in the phenol hydroxylation of magnetically separable CuFe2O4–reduced graphene oxide. Industrial & Engineering Chemistry Research. 2014;53(32):12566-74.
34. Cong HP, He JJ, Lu Y, Yu SH. Water-soluble magnetic-functionalized reduced graphene oxide sheets: in situ synthesis and magnetic resonance imaging applications. Small. 2010;6(2):169-73.
35. Fu M, Jiao Q, Zhao Y. Preparation of $NiFe_2O_4$ nanorod–graphene composites via an ionic liquid assisted one-step hydrothermal approach and their microwave absorbing properties. Journal of Materials Chemistry A. 2013;1(18):5577-86.
36. Baythoun MS, Sale FR. Production of strontium-substituted lanthanum manganite perovskite powder by the amorphous citrate process. Journal of Materials Science. 1982;17(9):2757-69.
37. Uddin ME, Kim NH, Kuila T, Lee SH, Hui D, Lee JH. Preparation of reduced graphene oxide-NiFe2O4 nanocomposites for the electrocatalytic oxidation of hydrazine. Composites Part B: Engineering. 2015;79:649-59.